Journal of Mining and Environment (JME) Vol. 16, No. 1, 2025, 143-159

Shahrood University of Technology

Journal of Mining and Environment (JME)

Journal homepage: www.jme.shahroodut.ac.ir

Iranian Society of Mining Engineering (IRSME)

A Proposed New Precambrian Skarn Deposits in the Arabian Shield

Eid R. Abo-Ezz[1,2], El Sayed I. Selim[1,3], Hatem Aboelkhair[3,4], and Haytham Sehsah[3*]

1. Department of Physics, College of Science and Humanities, Prince Sattam Bin Abdulaziz University, 11942, Al-Kharj, Saudi Arabia
2. Geophysics Department, Faculty of Science, Cairo University, Giza, P.O. 12613, Egypt
3. Faculty of Science, Geology Department, Damietta University, New Damietta City, 34517, Egypt
4. Center of Space Research and Applications (CSRA), Damietta University, New Damietta, Egypt

Article Info

Received 15 June 2024

Received in Revised form 16 July 2024

Accepted 4 August 2024

Published online 4 August 2024

DOI: 10.22044/jme.2024.14659.2769

Keywords

Neoproterozoic Skarn
Murdama carbonate
Causative plutons
Arabian-Nubian shield
Redox state of the magma

Abstract

The bimodal hypsometry of the Arabian-Nubian Shield in the Neoproterozoic triggered the formation of post-amalgamation marine bains in the low-stand terranes of the Arabian shield (AS). The carbonate successions in the extraordinary marine basins in the AS are intruded by granite plutons of different causative types, with major shear zones pathways. Therefore, the conditions for the formation of skarn deposits are mature at the contact of the carbonate succession with the causative granite plutons. Multidisciplinary approaches including ASTER data, Magnetic data, and geochemical data have been applied to the Murdama basin to locate the promising areas for skarn deposits. The Murdama basin has contrasting magnetic anomalies of different intensity at the contact between the Murdama limestone and the post-Murdama causative batholiths; significant magnetic anomalies exist at the contact with the Idah causative magmas. Lineaments related to the Najd fault system (NFS) exist eastward, where calc-silicate alteration-related minerals were evolved, with no clues for penetrative effect for such alteration activity along pathways related to the fracture system or at contact with the Abanat suite. Different spectral mapping techniques, including Spectral Information Divergence (SID), Spectral Angle Mapper (SAM), and Constrained Energy Minimization (CEM) confirm that the Idah suite is the predominant causative magma in the study area with highly evolved calc-silicate alteration-related minerals, such as wollastonite, garnet, and pyroxene. Meanwhile, The Idah suite has been identified as the main causative magma for other reduced skarn localities that have been recorded from the Murdama basin, i.e. the Qitan and An Nimriyah South. Alteration related mineral zones of kaolinite, chlorite, muscovite, and hematite are evolved alongside with calc-silicate minerals at the contact bewteen Idah suite, and the Murdama carbonate member. The geochemical data suggests reducing effect for the Idah suite at the contact between the Murdama carbonate succession and Idah plutons. These preliminary results of this study need detailed field investigations and geochemical explorations for the proposed skarn deposits in the Neoproterozoic molasse basins of the AS.

1. Introduction

Skarn deposits are important sources for elements that are significant for green economy transition, including high-technology tools, defense system equipment, renewable green energy, and transportation [1-3]. There are important factors controlling the distribution and constraining the formation of skarn deposits, including the type of causative magma and its physio-chemical conditions [4, 5], the fluid circulation pathways [6, 7], the distance from the causative magma [7], and the depth at which the skarn dposit had formed [8, 9]. Therefore, the type of skarn-related metals depend on the magma fractionation, and the redox conditions for the causative magma and country rocks [9].

The Neoproterozoic Arabian-Nubian Shield (ANS; Figure 1) had a contrasting hypsometry during the amalgamation of Gondwana

Corresponding author: Haytham_sehsah@du.edu.eg (H. Sehsah)

supercontinent c. 630 Ma, with lowstand eastern tract of the Arabian shield (AS) [10]. Therefore, extraordinary Gondwana post-amalgamation marine basins exist within the AS, intruded with different granite types.

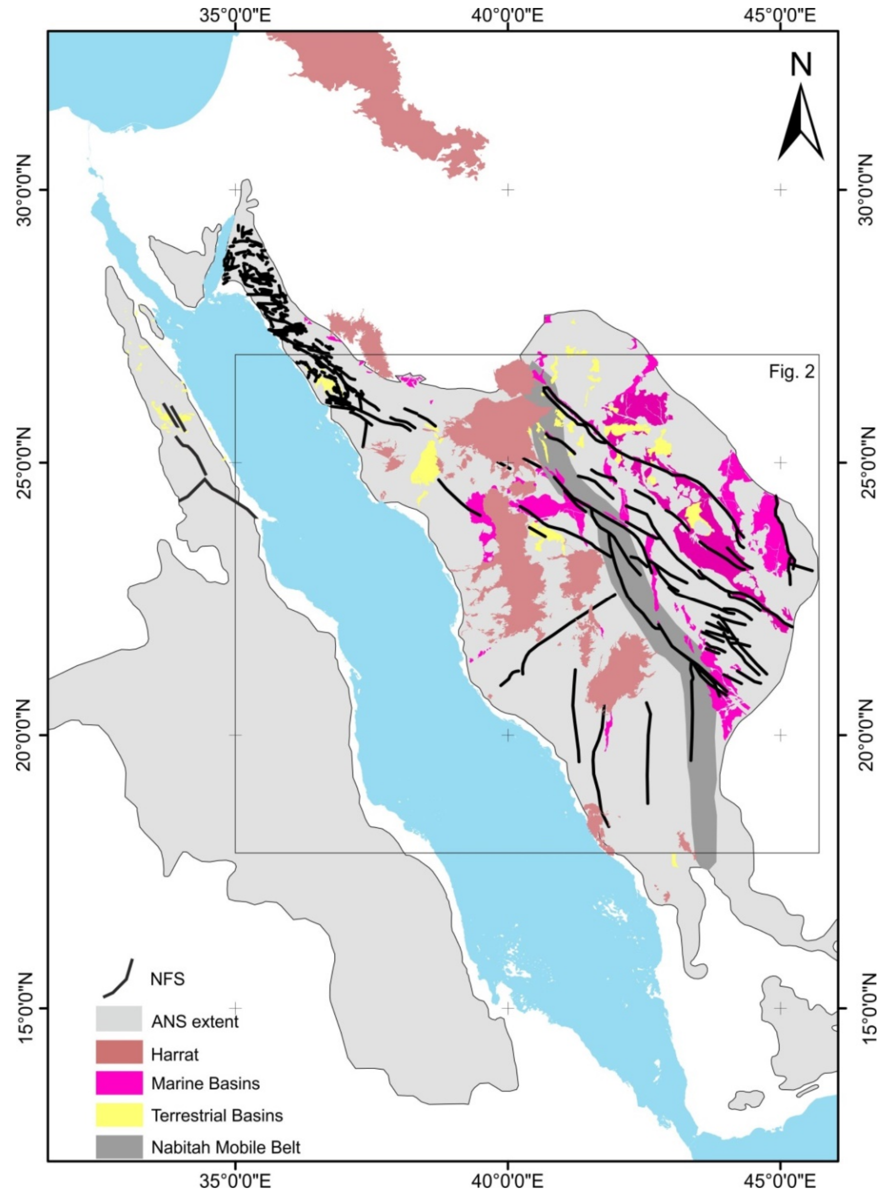

Figure 1. Different types of post – amalgamation basins in the Arabian – Nubian Shield (ANS), and the Najd fault system (NFS) [10-12]. Post-amalgamation marine basins exist in the eastern part of the Arabian shield (AS), where the Murdama basin (~ 72,000 km^2) is the largest molasse basin in the ANS.

Volcanosedimentary arc-related skarn deposits exist predominantly in the AS, including Al-Madhiq calcic type, Bahrah garnetiferous type, Jabal Ash Shumt [13], [14], [15]. Other localities for the volcanosedimentary arc-related skarns include Al Amar, Hamra, As Safra, Bi'r Ash Shumt, and Jabalul Hamat (Table S1). Meanwhile, few localities exist in the post-amalgamation basins, including Jibal Qitan, An Nimriyah South, and Kirsh skarn (Figure 2). Jibal Qitan garnetiferous-type skarn deposits exist at the contact between the Qitan causative granite and the Murdama limestone member [16]. Sn – W mineralization exposed at the surface in Qitan skarn locality, with possibility for potential subsurface mineralization at the contact between causative plutons and the Murdama group limestone [16]. Different post-Murdama causative granite types intrude the Murdama carbonate, so these intrusive contacts are promising areas for the skarn deposits.

The ASTER data usage include the lithological mapping of different rock units, and exploration of mineral alteration zones [17], including skarn deposits [18-21], porphyry-type deposits [22-26], volcanogenic massive sulphides [27]. Moreover, ASTER data were applied to identifying minerals, including quartz, and carbonate [28], and the iron oxides [29]. Potential field data, such as magnetic data were used for mapping lineament, [30-32], following the deep-seated structure [32, 33], and estimating the depth of structural elements and lithological units [34]. Furthermore, magnetic data has been applied for estimating the depth to the basement and the thickness of sedimentary cover [35], and the exploration of different ore deposits [30, 36, 37].Thus, magnetic data has been used for locating skarn deposits [38, 39].

It is important to undertake such study with multidisciplinary approach using geologic data, potential data analyses, ASTER data, and geochemical database to explore the possibility of skarn deposits in the post-amalgamation extraordinary marine basins – e.g. Murdama basin – to locate the source for irreplaceable sources for economic minerals in highly promising areas.

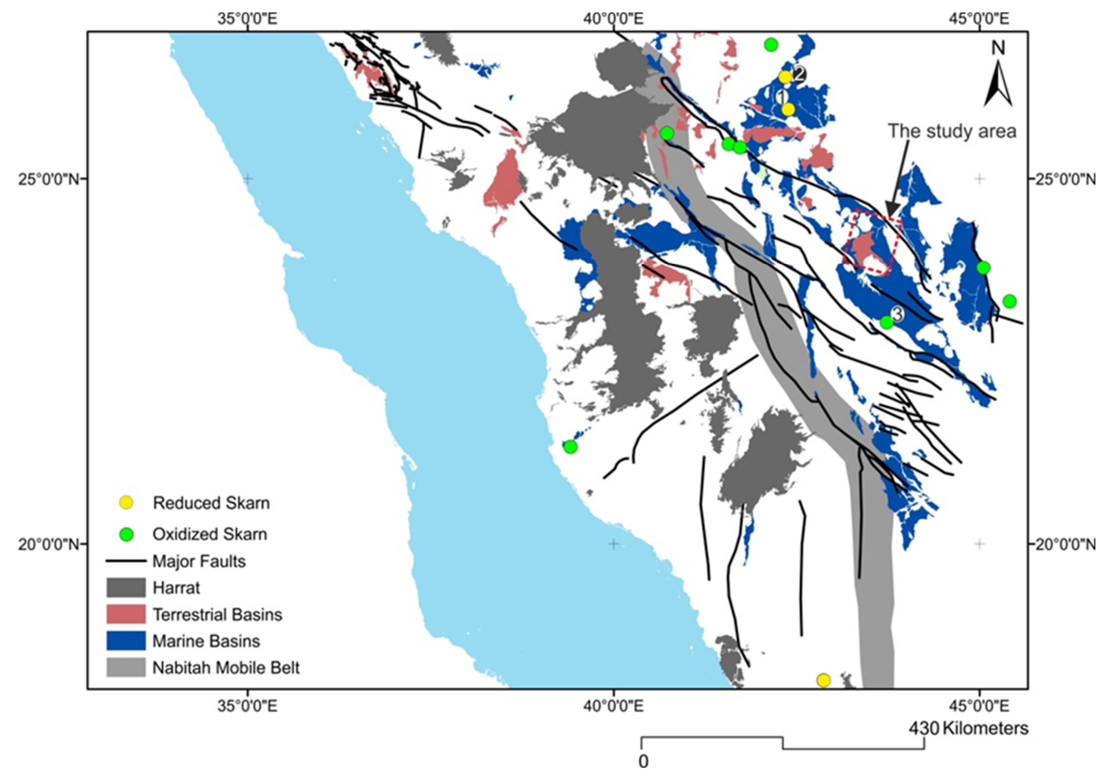

Figure 2. Skarn deposit locations in the Arabian shield (AS) from [13-16, 40-44]. Overall, the arc-related skarns are oxidized except for Al Madhiq. Meanwhile, three localities were recorded from the Murdama basin (1-3), namely Qitan (1), An Nimriyah South (2), and Kirsh (3). Qitan and An Nimriyah are reduced, and both of them are related to Idah causative plutons, while the Kirsh oxidized skarn is triggered by the Al Khushaymiyah suite.

2. The Geologic setting of Murdama basin

The Murdama post-amalgamation basin covers ~ 72000 km^2 in the Afif tract [11]. The Murdama basin is the largest post-amalgamation marine basin in the ANS, with a thick volcanosedimentary sequences, that lies unconformably above the pre-ANS Khida terrane at at the eastern boundary, covered unconformably with Cenozoic sedimentary cover to the SE [10]. Afif formation on the base of Murdama basin consists of calc-alkaline volcanic rocks of different composition, while the Murdama calc-clastic sedimentary sequence lies at the and the Afif formation on the top of the basin [11, 12]. The pre-Murdama Cryogenian rocks include both volcanosedimentary formations, i.e. Dhiran, Nafi, Hillit, Dhukhnah gneiss, Rika, Tays, Kabid formations, and granitoid suites of Khishaybi, Nasaf, Jidh, Labab and Kilab complexes, Suwaj, and Surayhah complex. The post-Murdama volcanosedimentary groups include Jibalah, Jurdhaiya, and Ediacaran rhyolite. Meanwhile, the basin is intruded by post-Murdama causative suites, including Al Khushaymiyah, Idah, Abanat, Ruwaydah, and Gharamil granite, Uraynibisuite, and Haml alkali feldspar granite.

Najirah volcanic arc granite has been emplaced in an active continental margin [45], and is exposed in Ad Dawadimi terrane as two large batholiths. The Najirah granite underlies the Abt formation, with no direct contact with the Murdama limestone. Najirah granite pre-dates the Abt formation, but both of them are intruded by the Ar Ruwaydah granitoids. The Idah suite exists in Ha'il and Afif teranes, and is composed of small post-orogenic alkli granite plutons [45], that intrud the northern part of the Murdama post-amalgamation basin, but this suite is absent in the southern part of the basin. Al Khushaymiyah complex post-dates the Murdama basin, and is exposed only in Afif terrane, with size increasing southward and intruding the central and southern parts of the basin.

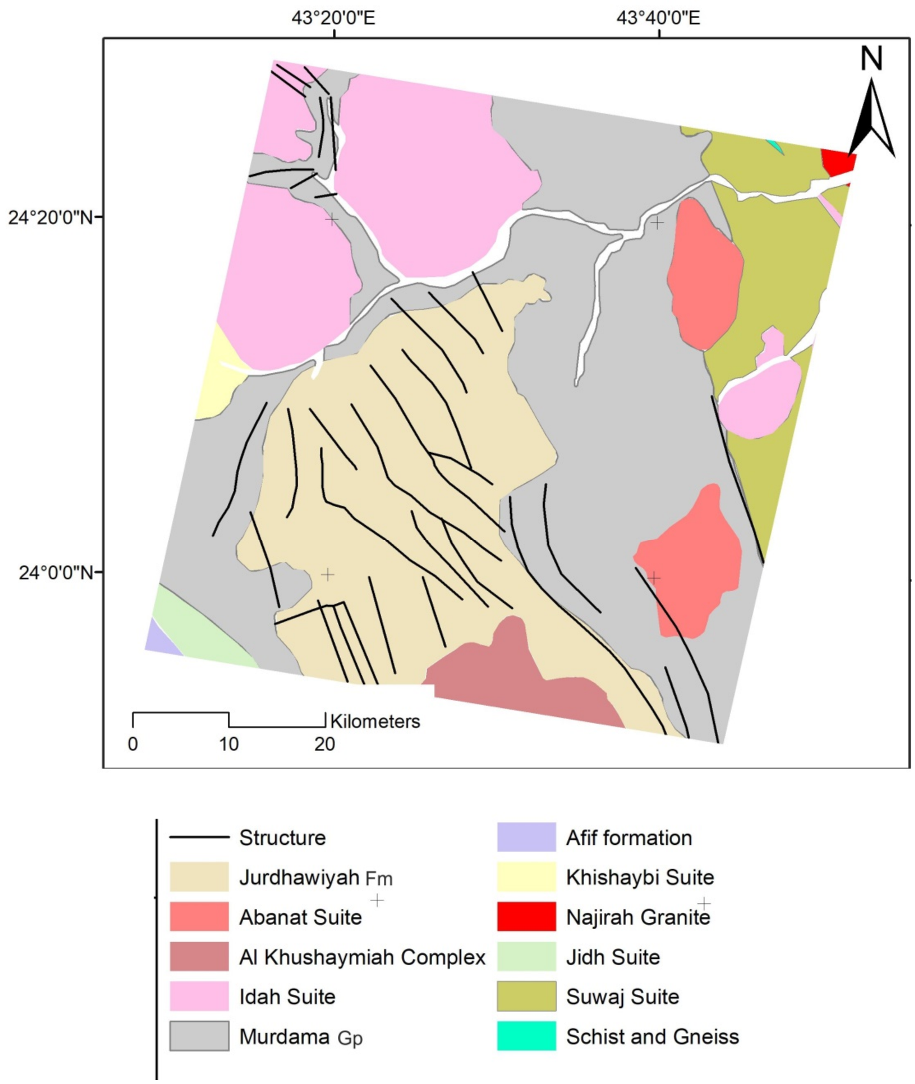

Figure 3. Geologic map of the study area after [11, 12]. Post-Murdama intrusions include the Idah suite, Al Khushaymiyah suite, and Abanat suite, where there is no direct contact between the Murdama group and the Al Khushaymiyah. Meanwhile, the Idah suite intruded the Murdama group, and this suite is the causative pluton for the reduced skarns recorded northward in the Murdama at Qitan and An Nimriyah South.

The Abanat plutons and Khishaybi batholiths are post-Murdama granite that intrudes the northern half of the Murdama basin, (Figure 3. The Murdama post-amalgamtation basin is composed of younger volcanosedimentary successions at the base of the basin in the west to marine successions at the eastern margin [10]. Therefore, skarn deposits exist mainly in the eastern terranes of the AS, and the fracture system related to the Najd fault system (NFS) controls the wall rock conditions. The NW structurally controlled framework of the mineral deposit zones is attributed to the NFS that controlled the circulation of hydrothermal fluids, and the emplacement of post-Murdama causative granite magmas. However, there are different phases of post-orogenic granites, but the Al Khushaymiyah and Idah suites are the main causative suites for the skarn ore deposits in the Murdama basin (Table S1). The Idah suite is the causative magmas for the reduced skarn types in Jibal Qitan, and An Nimriyah South r, while Al Khushaymiyah plutons are the causative source for the oxidizing skarn deposits at Kirsh in the Murdama basin (Figure 2; Table S1). Therefore, the contact between the causative plutons of the Idah suite and Al Khushaymiyah complex and the Murdama group is proposed to be a favored locality for skarn deposits.

3. Methodology

3.1. Magnetic data

The variation in the magnetic anomaly is caused by the lateral variations in the crust [46], with contributions from shallow and deep sources. Therefore, magnetic anomalies are significant to delineate different structural elements and map them at different crustal levels [33, 47-50]. Four advanced processing techniques were used to interpret the magnetic data, and map the fracture framework that facilitate the circulation of the hydrothermal fluids. The fast Fourier transformer's conversion was applied for the corrected data to convert the space domain into a frequency domain [51]. The four advanced techniques used in this study include Reduction to the pole, regional-residual separation, tilt derivatives, and analytical signal.

3.1.1. Reduced to the pole (RTP)

The reduced to the pole (RTP) tansformation of total magnetic intensity map is used to reduce the effect of latitudinal dipolar effect, using the inclination and declination angle values of 34.24 and 2.71, respectively. Few anomalies changed their orientation after the RTP transformation, and the RTP magnetic map does not diverge from the total intensity magnetic map.

3.1.2. Analytical signal technique

the analytical signal (AS) technique was applyed to get more information about the basement depth and subsurface border structural elements above the borders of the magnetic sources. The AS technique assumed that the structural border trends include geologic contact, faults, dike, and horizontal structures [52-54].

The AS is expressed as in its general form as follows [52];

$$AS = \sqrt{dx * dx + dy * dy + dz * dz}$$

where, dx, dy, dz are the vertical and horizontal derivatives of the magnetic field.

3.1.3. Tilt derivative technique

Tilt derivative (TDR) method is used to enhance the detection of subsurface structural lineaments and map the basement contact depths. The anomaly source was considered to be a 2D vertically buried contact (2D) [55], and depend on the vertical and horizontal derivatives of the magnetic field over the geologic boundary. Nabighian (1972) provides an equation for the horizontal and vertical derivatives of the geologic contacts at h = 0 and at a vertical depth of zc :

$$\frac{\partial M}{\partial h} = 2KFc^{\frac{zc}{h^2+zc^2}} \text{ and } \frac{\partial M}{\partial h} = 2KFc^{\frac{h}{h^2+zc^2}}$$

where h and Z are locations of the horizontal and vertical geologic contact, respectively, and K is the susceptibility contrast. Substituting the above derivative terms into the tilt equation and assuming a reduced to the pole magnetic field [55], it can be shown that,

$$\theta = \tan^{-1}\left[\frac{\frac{\partial M}{\partial Z}}{\frac{\partial M}{\partial h}}\right] \text{ and } \theta = \tan^{-1}\frac{h}{Zc}$$

According to this equation, contact-like geologic structures can be defined by the location (h = 0) and depth (half the physical distance between 45 contours) of the magnetic tilt angle contours [55].

3.1.4. Regional-Residual separation

The Butterworth filter was applied to extract the regional low (deep-seated magnetic sources) and residual (shallow-seated magnetic sources) components from the observed total intensity magnetic measurements using the Geosoft, 2015.

3.2. Remote Sensing Data and techniques

The images from ASTER's AST_L1B and AST_07XT products were retrieved via NASA's Land Processes Distributed Active Archive Center (LPDAAC). These images were acquired on

December 04, 2002, at 07:48:29 am with no cloud cover (0.0%), and underwent processing using (EXILIS ENVI 5.3) software. This process is aimed at geological and alteration mapping. Within the study area, a range of spectral mapping techniques including Spectral Information Divergence (SID), Spectral Angle Mapper (SAM), and Constrained Energy Minimization (CEM) were applied for analysis. The most economically promising minerals are primarily linked to alteration zones. Through field geological investigations, it was found that these zones have a relatively restricted spatial presence. As a result, conventional processing tools struggle to effectively distinguish them. Consequently, there is a necessity to differentiate the minerals connected to these alteration zones by employing more precise spectral classification tools such as SID, SAM, and CEM. Spectral Information Divergence (SID) employs a divergence metric to compare pixels with reference spectra. When the divergence is minimal, it suggests similarity between pixels. Conversely, if the divergence surpasses the maximum threshold, classification of the pixels won't occur (Chang, 1999). SAM, as an automated classification method, compares image spectra with known spectra or training classes. It calculates the spectral angle between the image spectrum (representing an unknown material) and the reference spectrum (representing a known material), treating them as vectors in an n-dimensional spectral space, where n represents the number of bands (Kruse et al., 1993). On the other hand, the CEM technique enhances the response of the target spectrum while minimizing the response of all other features, treating them as an unidentified background (Ren et al., 2003). In this study, the SID, SAM, and CEM techniques were utilized on the VNIR-SWIR stack datasets to distinguish alteration zones within the study area. The spectra from the JPL library were adjusted to correspond with the ASTER VNIR-SWIR spectrum. These mapping techniques were employed to map alteration minerals such as wollastonite, garnet, pyroxene, and epidote in the study area.

4. Results

4.1. Magnetic anomalies and fluid pathways framework

The total magnetic intensity map (TMI) with a scale of 1:25000 displays a sharp shift in magnetic anomaly, which could result from changes in lithology or topography, with contrasting magnetic anomalies of various amplitudes, wavelengths, and patterns. The magnetic anomaly values vary between -210 and 42 nT. The study area corners, and the central regions (Figure 4a) are home to magnetic anomalies of circular and elongated styles with highest amplitudes 42 nT. These elongated and circular anomalies reflect geologic body outlines, and the elongation shows the strike's direction of the geologic body [56]. The lowest value of magnetic anomaly -210 nT extrapolates thick sedimentary cover that exists above the center of the basin towards the southwest. The fault contact related to the NFS is characterized by a contrasting style of negative and positive magnetic anomalies.

The irregular bimodal distribution of magnetic anomalies reflects different lithological varieties and the contrast distribution of a dense sedimentary succession. The RTP map reflects the existence of a wide range of magnetic values (-227 to 120 nT). The highest magnetic value is 120 nT, which extend in northwest and southeast directions, while the lowest value -227 nT with NE-SW directions, exist in the central and southwest parts with NE-SW directions (Figure 4b). The granitic rocks have higher anomalies than the Murdama basin volcanosedimentary successions. Meanwhile, the granitic suits show contrasting anomalies, where the Abanat suite has relatively lower magnetic anomaly values than the Idah plutons, which have significantly higher magnetic anomaly values over the study area. Al Khushaymiyah complex anomaly is higher than the Abanat suite, and is similar to the Idah plutons, and there is a high anomaly at the eastern part of the Murdama basin near Al Khushaymiyah. The NW linear extension of this anomaly predicts the extension of this anomaly in the subsurface.

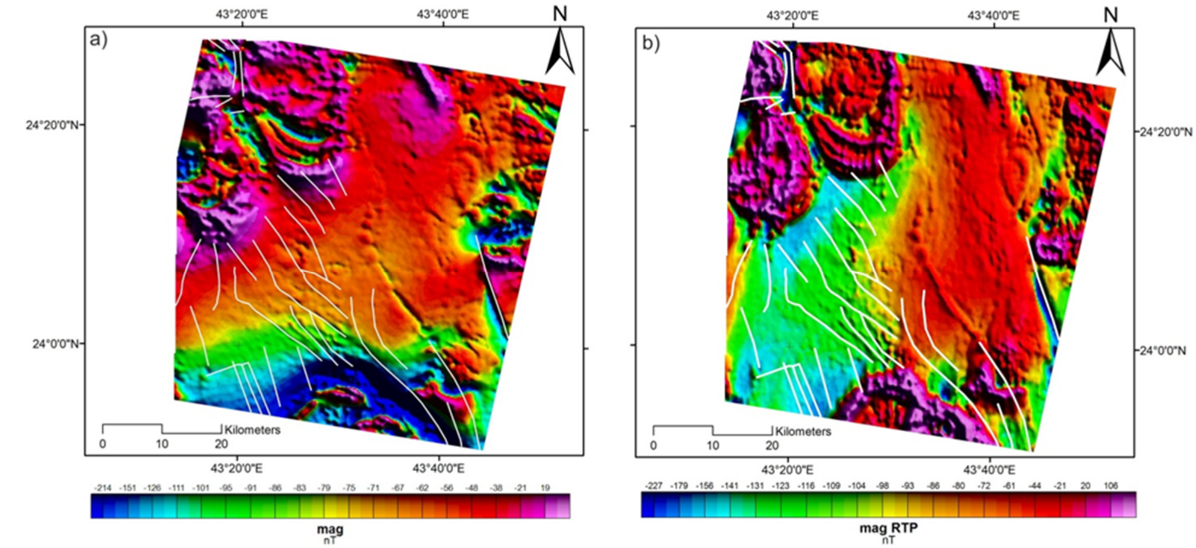

Figure 4 a) total intensity magnetic map for the northern part of the Murdama basin; b) reduced to the pole (RTP) map

The AS enhanced both the extent and direction of the magnetic anomalies along the contact of granitic plutons, where the Idah plutons and Al Khushaymiyah complex have higher boundary anomalies than other post-Murdama intrusive suites. Meanwhile, the AS technique unraveled the presence of a structurally controlled basement anomaly underneath the eastern domain of the Murdama basin. The AS map revealed the existence of linear border anomalies with NW direction at the contact with the Suwaj suite and to the SW of the Idah suite plutons in the eastern part of the study area.

The TD map revealed the existence of curved to circular magnetic anomalies at the contacts with the Idah and Abanat plutons, and Al Khushaymiyah complex. The eastern part of the basin is controlled by NW subsurface lineaments pathways, and this may reflect shallow depth to the older basement, and the later NFS related magmatism. The deep-seated magnetic anomaly sources derived from the regional separation technique have NE-SW direction parallel to the terranes boundary between Ha'il and Afif domains, so the source of the deep-seated anomaly may be inherited from the older activities of the arc-related basements. Granitic suite contacts are the source for the shallow-seated magnetic anomalies, with extension of the Al Khushayimah complex underneath the thin sedimentary cover of Jurdahawiyah below the eastern part of the basin. The Idah and Abanat suites have higher anomalies at the eastern boundary of the Murdama basin.

The AS map (Figure 5a) gives high resolution detection for the edges of the magnetic anomaly sources). The effect of the NFS with NNW-SSE trend is significant in the study area. The TD map (Figure 5b) provides the dominant trend more simply and plainly than the RTP map, and confirms the predominant effect of the NFS with a significant NNW-SSE structural trend.

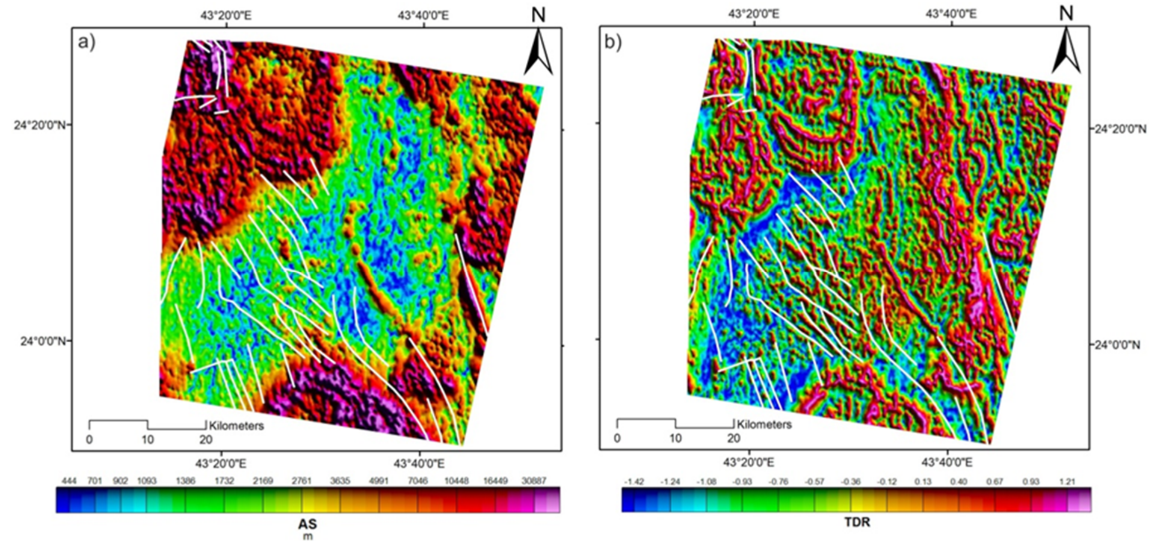

Figure5 a) Analytical signal (AS); b) tilted derivative analyses for the RTP anomaly.

The subsurface structural trends based on different techniques, such as the RTP map (Figure 4b), and the regional (Low-Pass) magnetic map (Figure 6a), are compatible with no significant difference. Numerous magnetic anomalies of long-wavelength and low-frequency with various patterns, magnitudes, and trends may be seen on the low-pass magnetic map (Figure 4a). The structure styles and the deep crustal sources could be identified from the shape and frequency of these anomalies. The regional magnetic map reflects the existence of NE–SW and NNE–SSW trending faults. These subsurface lineament trends are related to the NFS framework.

Many contrasting high and low magnetic anomalies exist on the residual (high-pass) magnetic map (Figure 6b). These anomalies are located in center and western regions, and there are linear magnetic anomalies induced by shallow-seated structural lineaments. NE–SW, N–S and NW–SE residual anomaly trends occupy the southern and western domains of the study area.

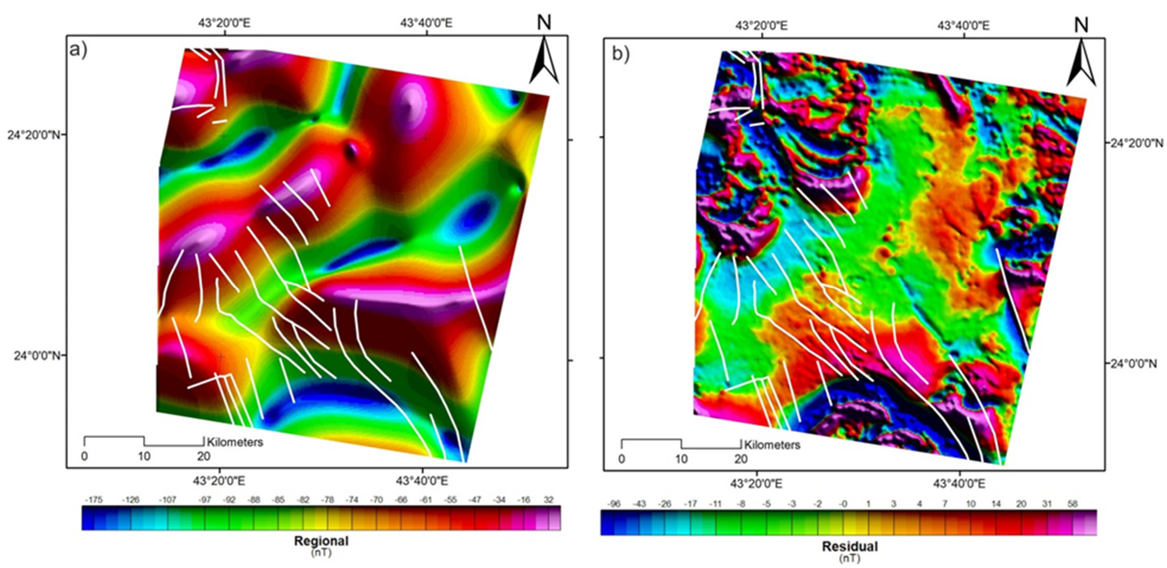

Figure6 Regional – residual separation a) regional separation; b) residual separation.

4.2. Types source of alteration minerals

Skarns are derived from the interaction between the hydrothermal fluids with the carbonate rocks as a result of intruding felsic causative magmas to produce varieties of calc-silicate minerals, including wollastonite, garnet, and pyroxene [57-60]. Therefore, skarns are always found near igneous causative magmas, and along fractures and shear zones pathways [61], based on the source and type of the hydrothermal fluids [62], with evidence for shallow geothermal systems at shallow crustal levels [63, 64]. The existence of wollastonite suggests SiO_2 supersaturated causative intrusions, the Idah and Al Khushaymiyah suites being the main causative magmas for previously recorded skarn deposits in the basin. Wollastonite mineral mapping reveals its existence at the contact with Idah plutons at the upper left corner of the study area (Figure 7a). Although the NFS is the main pathway fractures network, there is no record for the calc-silicate alteration mineral zones in the central domain of the basin. The wollastonite exist only at the Idah suite contacts with the Idah suite, and this reflects the saturation of the magma with SiO_2, and this explains the existence of other skarn deposits at Qitan and An Nimriyah South at the contact of Idah suite causative magmas (Figure 2), (Table S1). The wollastonite is absent at the contact of Al Khushaymiyah complex (Figure 7a), because there is no direct surface contact with the Murdama group (Figure 3), but the higher magnetic anomaly suggests the existence of such contact in the subsurface.

Garnet is an important proximal indicator of metasomatized carbonate protoliths [2]. Garnet exists at the upper left corner of the study area, in association with the wollastonite (Figure 7b). Garnet exists at the same area of the wollastonite at the contact with the Idah suite, with no effect for the NFS fracture system on the distribution of the hydrothermal skarn deposits. Meanwhile, the tectonic contact between the basin and the Suwaj suite is barren of skarn calc-silicate minerals, including the garnet and wollastoniate, and there is no effect of Al Khushaymiyah complex on the Murdama basin (Figure 7b). Pyroxenes are a common distal indicator for the skarn deposits [2, 65].

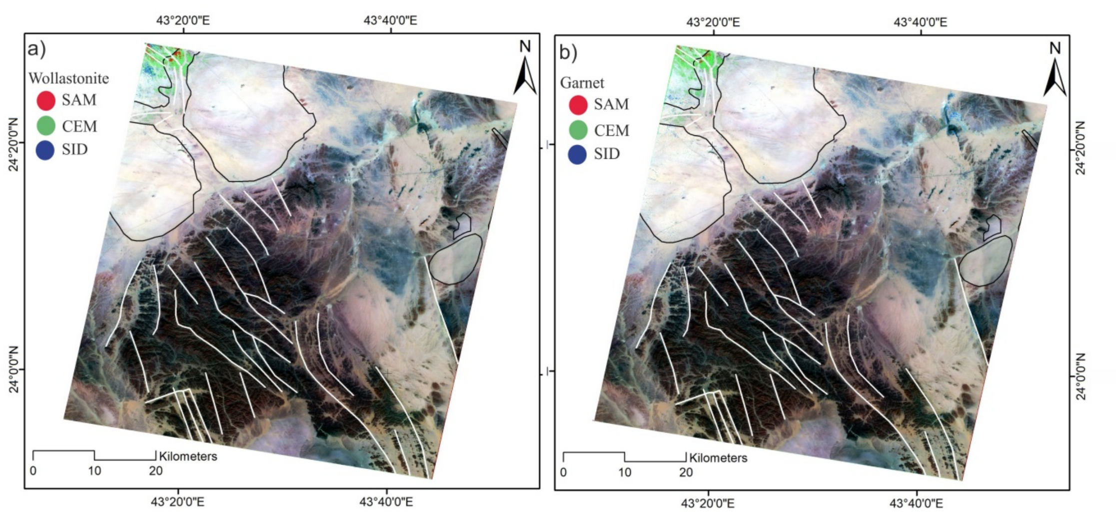

Figure 7 a) Wollastonite mineral zone; b) garnet mineral zone. Spectral Angle Mapper (SAM) is in red, Constrained Energy Minimization (CEM) is in green, and Spectral Information Divergence (SID) is in blue.

Pyroxene exists with other calc-silicate minerals in the northwestern corner of the study area, but with a relatively greater extent than other calc-silicate minerals away from the contact of the Idah suite (Figure 8a). The mapping of different calc-silicate alteration zones related to the skarn deposits in the investigated area confirms the distribution of the mineralization with the Idah suite. Therefore, the Idah plutons are the main causative magmas for the skarn deposits in the Murdama basin, with no effect for Al Khushaymiyah complex and the NFS fracture system. Meanwhile, the Idah suite is the causative magmas for other skarn deposits in the Murdama post-amalgamation basin at Qitan and An Nimriyah South (Table S1). Furthermore, the barren NFS fracture system suggests that the hydrothermal activity was derived from the Idah suite magmatic system. However, the Al Khushaymiyah complex is the causative magma for the Kirsh skarn (Table S1), it has no effect on the Murdama group, where there is no direct contact with the Murdama group. Meanwhile, the tectonic contact with the Suwaj suite is barren (Figure 8b).

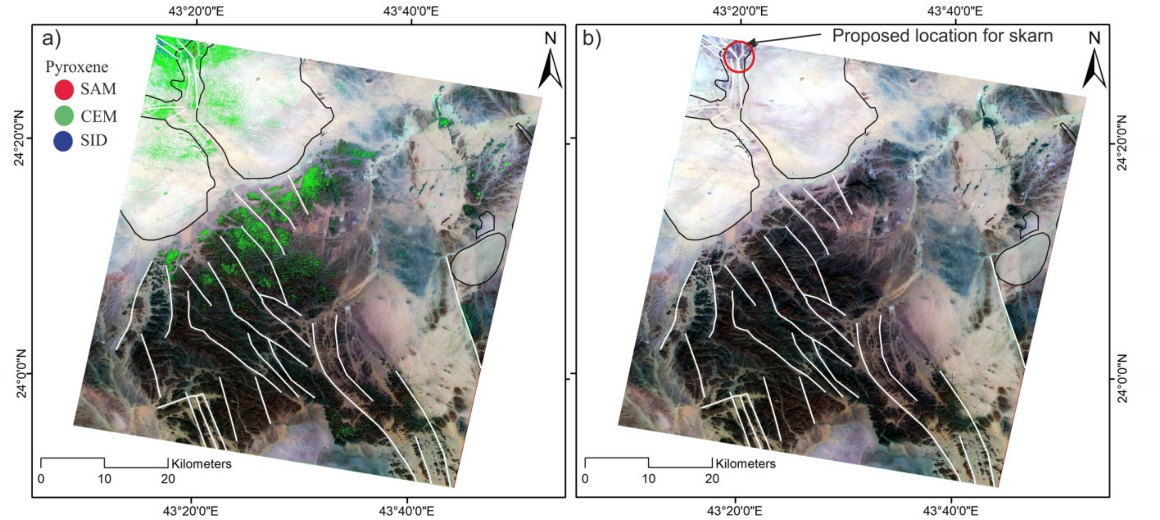

Figure 8 a) Clinopyroxene mineral zone; the colors as in Figure 7; b) the proposed skarn deposits at the contact between the Idah suite and the Murdama group, based on the integration of Spectral Angle Mapper (SAM), Constrained Energy Minimization (CEM), Spectral Information Divergence (SID), and the magnetic anomaly of the Idah suite.

The intersection points of faults and the intrusive contact are suggested as a promising areas for ore deposits related to hydrothermal fluid flux [66]. The depositional zone of the proposed skarn deposits (Figs. 7&8) are dissected by faults related to the NFS, and at the contact between the Murdama member and the Idah suite.

5. Mineralization types of the proposed skarn deposits

Different fractal, statical, and geochemical modeling techniques have been used to explore the distribution controls of ore deposits [67-72]. The redox state for the protolith and the causative plutons controls the type of skarn deposits mineralization. Nickel plate mine in British Columbia is an example for reducing conditions for the protolith and the wall rock, so Au is the common ore deposit in such conditions [73]. In the Cu skarn prospect of the Philippines, the conditions of skarn ore deposits are oxidizing with more garnet [74-76]. The conditions of the magma control the type of skarn-related ore that is being evolved, Au and Sn exists in reducing conditions, but their association in the same magmatic system is rare, because Au associates mafic magma, while Sn exists in felsic magmatic systems [7]. The distribution of Cu – Mo deposits favor oxidized magma, but Mo exists in less oxidized systems and highly fractionated felsic magmas, while Zn – Pb exists in contrasting conditions of various degrees of fractionation.

Volcanosedimentary arc-related successions skarn deposits are the predominant type in the AS, except for few localities in Jibal Qitan, An Nimriyah South, and Kirsh (Figure 2; Table S1). Meanwhile, the Murdama basin is intruded with different types of granite causative magmas, so the contact between the causative post-Murdama granite and the Murdama member are suitable locations for skarn deposits. Meanwhile, Al Khushaymiyah complex and Idah suite are the main causative magmas for the skarn ore deposits in the Murdama post-amalgamation basin (Table S1), including Jibal Qitan and An Nimriyah South reduced skarns related to the Idah causative plutons (Figure 2; Table S1), with Sn – W mineralizations [16]. However, the Al Khushaymiyah complex is an oxidizing causative magma, and this complex induced the Kirsh oxidized skarn (Table S1). The redox state of the post-Murdama plutons, based on the $Fe^{3+}/Fe2^{+}$ ratio Fe_2O_3 / (Fe_2O_3 + FeO) vs. SiO_2 diagram after [3], confirms the reducing state for the Idah magmas and an oxidizing state for Al Khushaymiyah complex (Figure 9). In the area under investigation, the Idah suite intrudes the Murdama limestone, while Al Khushaymiyah complex has no direct contact with the Murdama group, so reduced skarn at the contact with the Idah suite are proposed to exist (Figure 8b), based on the extension of the magnetic anomaly, the extent of the calc-silicate mineral alteration zones, and the redox state of the Idah suite.

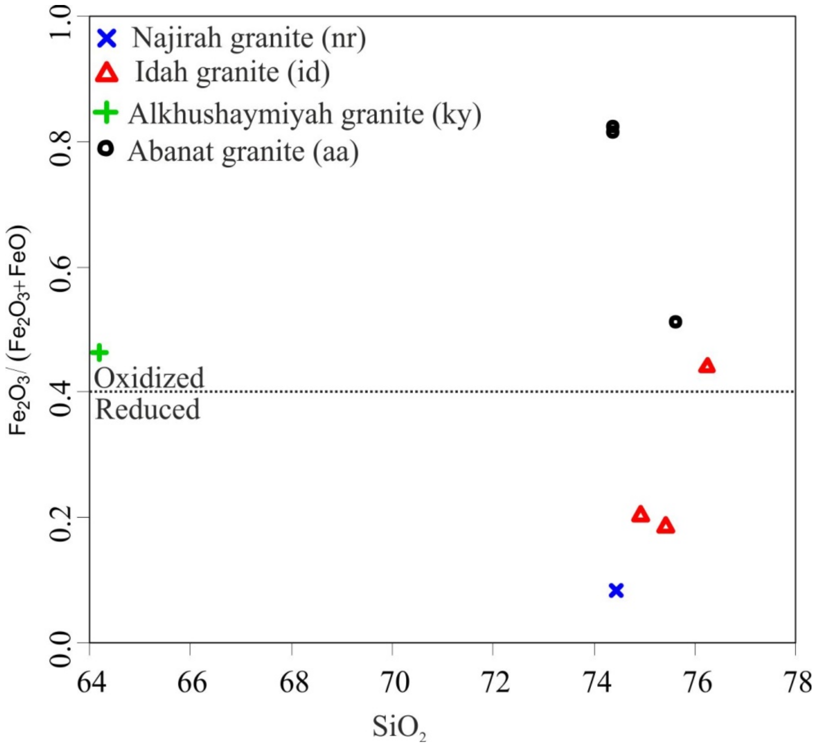

Figure 9. Redox state for the post – Murdama granite causative magmas; the geochemical analyses from [45]; for the complete analyses refer to (Table S2), where analyses with Fe_2O_3T were excluded from the plotting. The redox index based on the Fe_2O_3 / (Fe_2O_3 + FeO) vs. SiO_2 after [3]

The metal associations of skarn deposits are classified under four categories: 1) Mo – W – Cu – Zn – Pb, and this type exists in oxidized, moderate to strong fractionation condition [7, 77]; 2) Fe – Cu (±W) – Au – Zn – Pb, and this category favors oxidized, weak to moderate fractionation condition [7, 78]; 3) Sn – W – Zn – Pb, and this type occurs in reduced, strongly fractionation environment [1]; 4) Au – Zn – Pb, and this association exists in reduced, weak to moderate fractionated conditions [7]. Reduced skarn deposits in the Murdama basin induced by the Idah suite causative magma are enriched in Sn – W mineralizations, i.e. Jibal Qitan garnetiferous-type skarn deposits [16]. Based on the integration of three different datasets; the preliminary results suggest the existence of reduced skarn deposits in the Murdama basin at the contact with Idah causative magma. The Precambrian limestone member in the marine bains of the AS are promising areas for skran deposits, and more geologic and geochemical investigations are required.

6. Discussion

The AS has voluminous post-amalgamation mixed and marine basins including the Murdama basin, most of the recorded skarn deposits in the ANS are arc–related volcanosedimentary successions, except for few localities in the Murdama marine basin (Figure 2). During the Cryogenian c. 650 Ma, the ANS experienced the transition from arc-related deposition systems to deposition in different types of post-amalgamation basins [10, 12]. Late Neoproterozoic (650 – 542 Ma) marine basins are dominant in the AS, with an average thickness of c. 4 km [10].

Late Ediacaran post-Murdama granitic plutons intrude the marine basins. These suites include the Al Khushaymiyah complex, Idah, Abanat, and Ruwaydah suites, and the Gharamil granite. Skarn deposits are well-developed at the intrusive contact between the carbonates protolith and late intrusions [2, 3, 9]. Meanwhile, the post-amalgamation basins variably experienced brittle deformation style with common cleavage, fractures and lineation, and such fracture systems are the pathways for hydrothermal fluid activities. Meanwhile, both the Idah suite and Al Khushayimah complex are the main causative magmas for the skarn deposits in the Murdama marine basin at Qitan, An Nimriyah South, and Kirsh (Figure 2; Table S1). Therefore, skarn deposits were proposed to exist at the contact between these causative suites and the Murdama group. However, the mapping of calc-silicate alteration zones reveals the existence of skarn-related minerals at the contact with the Idah suite and the Murdama limestone, with no record for the calc-silicate indicators at the contact of Al Khushayimah complex (Figs. 7 & 8). Meanwhile, the contact of the Al Khushayimah complex is barren, because it intrudes the Jurdhawiya formation with no direct contact with the Murdama formation (Figure 3). The barren NFS fracture system suggests that the source of hydrothermal fluids was the Idah suite magmas, because the detected calc-silicate alteration zones exist at the contact of the Idah suite with the Murdama group.

The Idah post-Murdama causative magmas are the main trigger for the skarn deposits in the Murdama basin, including Jibal Qitan, An Nimriyah South, and Kirsh skarn (Figure 2). Jibal Qitan garnetiferous-type skarn deposits exist at the contact between the Qitan causative granite and the Murdama limestone member [16]. Sn-W mineralization is exposed at the surface in Qitan skarn locality, with possibility for potential subsurface mineralization at the contact between causative plutons and the Murdama group limestone [16]. Different post-Murdama causative granite types intrude the Murdama carbonate, so these intrusive contacts are promising areas for the skarn deposits. However, different causative magma types intrude the Murdama basin, including the Idah, Al Khushaymiyah, and Abanat suites. There is no direct contact between the Murdama group and the Al Khushaymiyah, and the Abanat suite intudes the Murdama carbonate barren sucessions. The fluid structural framework subsystem requires intersection with the causative magma contact [66]. The Idah suite is the only post-Murdama causative magma in the study area that intrudes the Murdama member, so a new localities for the reduced skarn deposits have been proposed.

7. Conclusions

The integration between potential field magnetic data, ASTER, and the geochemical database give the following conclusions:

1. The Idah plutons have the highest magnetic anomalies than other post-Murdama intrusive suites.
2. The calc-silicate mineral alteration zones exist at the contact of the Idah suite, without any record for such alteration zones along fracture systems related to the NFS.
3. The intrusive contact between the Murdama member and the post-Murdama suites is barren. However, the Al Khushaymiyah complex, which caused the Kirsh oxidized skarn has no direct contact with the Murdama group.
4. The skarn mineral alteration zones in the study area was induced by the Idah suite, which has a reducing state. Meanwhile, this is confirmed by the reduced skarns at Jibal Qitan and An Nimriyah South, where both of them were induced by the Idah suite.

Acknowledgment

The authors extend their appreciation to the Deputyship for Research & Innovation, Ministry of Education in Saudi Arabia for funding this research work through project number (IF-PSAU-2021 /01/18782).

References

[1]. W.-C. Jiang, H. Li, R. Mathur, and J.-H. Wu, "Genesis of the giant Shizhuyuan W–Sn–Mo–Bi–Pb–Zn polymetallic deposit, South China: constraints from zircon geochronology and geochemistry in skarns," *Ore Geology Reviews,* vol. 111, p. 102980, 2019.

[2]. L. D. Meinert, "Application of skarn deposit zonation models to mineral exploration," *Exploration and mining geology,* vol. 6, pp. 185-208, 1997.

[3]. L. D. Meinert, "Compositional variation of igneous rocks associated with skarn deposits-chemical evidence for a genetic connection between petrogenesis and mineralization," *Mineralogical Association of Canada Short Course Series, vol.,* vol. 23, pp. 401-418, 1995.

[4]. H. Legros, P. Lecumberri-Sanchez, V. Elongo, O. Laurent, H. Falck, E. Adlakha*, et al.*, "Fluid evolution of the Cantung tungsten skarn, Northwest Territories, Canada: Differentiation and fluid-rock interaction," *Ore Geology Reviews,* vol. 127, p. 103866, 2020.

[5]. Q. Shu, Z. Chang, Y. Lai, X. Hu, H. Wu, Y. Zhang*, et al.*, "Zircon trace elements and magma fertility: insights from porphyry (-skarn) Mo deposits in NE China," *Mineralium Deposita,* vol. 54, pp. 645-656, 2019.

[6]. L. Nie, G. Cai, J. Lin, F. Wang, Y. Cai, J. Fu*, et al.*, "Constrains of physical properties and geochemical characteristics of country rock on skarn tungsten mineralization: a case study of the Longjiaoshan-

Fujiashan skarn tungsten deposit in the Middle-Lower Yangtze River Metallogenic Belt," *Ore Geology Reviews,* p. 105032, 2022.

[7]. Z. Chang, Q. Shu, and L. Meinert, "Skarn deposits of China," *Society of Economic Geologists,* vol. Special Publication 22, pp. 189 - 234, 2019.

[8]. Z. Zhou, J. Mao, H. Che, H. Ouyang, and X. Ma, "Metallogeny of the Handagai skarn Fe–Cu deposit, northern Great Xing'an Range, NE China: Constraints on fluid inclusions and skarn genesis," *Ore Geology Reviews,* vol. 80, pp. 623-644, 2017.

[9]. L. D. Meinert, K. K. Hefton, D. Mayes, and I. Tasiran, "Geology, zonation, and fluid evolution of the Big Gossan Cu-Au skarn deposit, Ertsberg district, Irian Jaya," *Economic Geology,* vol. 92, pp. 509-534, 1997.

[10]. P. Johnson, A. Andresen, A. Collins, A. Fowler, H. Fritz, W. Ghebreab*, et al.*, "Late Cryogenian–Ediacaran history of the Arabian–Nubian Shield: a review of depositional, plutonic, structural, and tectonic events in the closing stages of the northern East African Orogen," *Journal of African Earth Sciences,* vol. 61, pp. 167-232, 2011.

[11]. P. R. Johnson, "Post-amalgamation basins of the NE Arabian shield and implications for Neoproterozoic III tectonism in the northern East African orogen," *Precambrian Research,* vol. 123, pp. 321-337, 2003.

[12]. P. R. Johnson, G. P. Halverson, T. M. Kusky, R. J. Stern, and V. Pease, "Volcanosedimentary basins in the Arabian-Nubian Shield: Markers of repeated exhumation and denudation in a Neoproterozoic accretionary orogen," *Geosciences,* vol. 3, pp. 389-445, 2013.

[13]. Z. Ahmed, "Composition of skarn grossular from Al-Madhiq area, SW Saudi Arabia," *Arabian Journal for Science and Engineering. Section B: Engineering,* vol. 27, pp. 3-16, 2002.

[14]. A. A. Surour and A. Moufti, "A new occurrence of garnetiferous skarn rocks in Saudi Arabia: a case study from Bahrah area, Jeddah–Makkah Al Mukaramah highway," *Arabian Journal of Geosciences,* vol. 4, pp. 879-897, 2011.

[15]. A. M. Moufti, "Mineralogy and Metamorphic Evolution of Jabal Ash Shumt Skarn Deposits, Saudi Arabia: An Example of Superimposed Metamorphism," *Journal of King Abdulaziz University: Earth Sciences,* vol. 24, 2013.

[16]. W. R. Miller and M. A. Arnold, "Results of a Geochemical Survey, Aban Al Ahmar Quadrangle, Sheet 25F, Kingdom of Saudi Arabia," US Geological Survey 2331-1258, 1988.

[17]. M. Abrams and Y. Yamaguchi, "Twenty years of ASTER contributions to lithologic mapping and mineral exploration," *Remote Sensing,* vol. 11, p. 1394, 2019.

[18]. T. Yajima, "ASTER data analysis applied to mineral resource exploration and geological mapping," *Nagoya University: Nagoya, Japan,* p. 77, 2014.

[19]. T. Cudahy, K. Okada, A. Cornelius, and R. Hewson, "Regional to prospect scale exploration for porphyry-skarn-epithermal mineralisation at Yerington, Nevada, using ASTER and airborne Hyperspectral data," *CSIRO Exploration and Mining Report,* 2002.

[20]. T.-T. Liu, Z.-W. He, X.-L. Cui, and H. Gao, "The strucuture of the model for skarn-type lead-zinc deposit based on ASTER data," *Xibei Shifan Daxue Xuebao/ Journal of Northwest Normal University(Natural Science),* vol. 48, pp. 100-105, 2012.

[21]. H. Moradpour, G. Rostami Paydar, A. B. Pour, K. Valizadeh Kamran, B. Feizizadeh, A. M. Muslim*, et al.*, "Landsat-7 and ASTER remote sensing satellite imagery for identification of iron skarn mineralization in metamorphic regions," *Geocarto International,* vol. 37, pp. 1971-1998, 2022.

[22]. Q. Chen, Z. Zhao, J. Zhou, M. Zeng, J. Xia, T. Sun*, et al.*, "New insights into the Pulang porphyry copper deposit in southwest China: Indication of alteration minerals detected using ASTER and WorldView-3 data," *Remote Sensing,* vol. 13, p. 2798, 2021.

[23]. S. Beygi, I. V. Talovina, M. Tadayon, and A. B. Pour, "Alteration and structural features mapping in Kacho-Mesqal zone, Central Iran using ASTER remote sensing data for porphyry copper exploration," *International Journal of Image and Data Fusion,* vol. 12, pp. 155-175, 2021.

[24]. Z. Wang, C. Zhou, and H. Qin, "Detection of hydrothermal alteration zones using ASTER data in Nimu porphyry copper deposit, south Tibet, China," *Advances in Space Research,* vol. 65, pp. 1818-1830, 2020.

[25]. S. Fakhari, A. Jafarirad, P. Afzal, and M. Lotfi, "Delineation of hydrothermal alteration zones for porphyry systems utilizing ASTER data in Jebal-Barez area, SE Iran," *Iranian Journal of Earth Sciences,* vol. 11, pp. 80-92, 2019.

[26]. B. Behbahanı, H. Haratı, P. Afzal, and M. Lotfı, "Determination of alteration zones applying fractal modeling and Spectral Feature Fitting (SFF) method in Saryazd porphyry copper system, central Iran," *Bulletin of the Mineral Research and Exploration,* vol. 172, pp. 1-14, 2023.

[27]. S. Rajendran and S. Nasir, "Characterization of ASTER spectral bands for mapping of alteration zones of volcanogenic massive sulphide deposits," *Ore Geology Reviews,* vol. 88, pp. 317-335, 2017.

[28]. B. W. Rockwell and A. H. Hofstra, "Identification of quartz and carbonate minerals across northern Nevada using ASTER thermal infrared emissivity data—Implications for geologic mapping and mineral

resource investigations in well-studied and frontier areas," *Geosphere,* vol. 4, pp. 218-246, 2008.

[29]. L. C. Rowan and J. C. Mars, "Lithologic mapping in the Mountain Pass, California area using advanced spaceborne thermal emission and reflection radiometer (ASTER) data," *Remote sensing of Environment,* vol. 84, pp. 350-366, 2003.

[30]. K. S. Essa, M. Munschy, M. A. Youssef, and E. E. D. A. H. Khalaf, "Aeromagnetic and radiometric data interpretation to delineate the structural elements and probable precambrian mineralization zones: A case study, Egypt," *Mining, Metallurgy & Exploration,* vol. 39, pp. 2461-2475, 2022.

[31]. M. Abdullahi, U. K. Singh, and R. Roshan, "Mapping magnetic lineaments and subsurface basement beneath parts of Lower Benue Trough (LBT), Nigeria: Insights from integrating gravity, magnetic and geologic data," *Journal of Earth System Science,* vol. 128, pp. 1-17, 2019.

[32]. A. M. Eldosouky, R. A. El-Qassas, L. T. Pham, K. Abdelrahman, M. S. Alhumimidi, A. El Bahrawy*, et al.*, "Mapping main structures and related mineralization of the Arabian Shield (Saudi Arabia) using sharp edge detector of transformed gravity data," *Minerals,* vol. 12, p. 71, 2022.

[33]. H. Sehsah, A. M. Eldosouky, and L. T. Pham, "Incremental Emplacement of the Sierra Nevada Batholith Constrained by U-Pb Ages and Potential Field Data," *The Journal of Geology,* vol. 130, pp. 381-391, 2022.

[34]. E. Abdelrahman, H. M. El-Arby, T. M. El-Arby, and K. S. Essa, "A least-squares minimization approach to depth determination from magnetic data," *pure and applied geophysics,* vol. 160, pp. 1259-1271, 2003.

[35]. E. Aboud, "Determination of sedimentary cover and structural trends in the Central Sinai area using gravity and magnetic data analysis," *Journal of Asian Earth Sciences,* vol. 43, pp. 193-206, 2012.

[36]. J. Yang, S. Liu, and X. Hu, "Inversion of high-amplitude magnetic total field anomaly: An application to the Mengku iron-ore deposit, northwest China," *Scientific Reports,* vol. 10, p. 11949, 2020.

[37]. M. Gobashy, M. Abdelazeem, and M. Abdrabou, "Minerals and ore deposits exploration using meta-heuristic based optimization on magnetic data," *Contributions to Geophysics and Geodesy,* vol. 50, pp. 161-199, 2020.

[38]. G. Martelet, E. Gloaguen, A. Døssing, E. Lima Simoes da Silva, J. Linde, and T. M. Rasmussen, "Airborne/UAV multisensor surveys enhance the geological mapping and 3d model of a pseudo-skarn deposit in Ploumanac'h, French Brittany," *Minerals,* vol. 11, p. 1259, 2021.

[39]. P. Gunn and M. Dentith, "Magnetic responses associated with mineral deposits," *AGSO Journal of Australian Geology and Geophysics,* vol. 17, pp. 145-158, 1997.

[40]. Z. Ahmed and M. M. Hariri, "Formation and mineral chemistry of a calcic skarn from Al-Madhiq, SW Saudi Arabia," *Geochemistry,* vol. 66, pp. 187-201, 2006.

[41]. P. L. Williams, "Reconnaissance Geology of the Samirah Quadrangle, Sheet 26/42 C, Kingdom of Saudi Arabia," US Geological Survey 2331-1258, 1984.

[42]. C. Hummel and A. O. Ankary, "Geology and mineral deposits of the Jabal ash Shumta quadrangle, Kingdom of Saudi Arabia," US Geological Survey 2331-1258, 1972.

[43]. B. Lemiere, N. Damanhori, and G. Baudet, "A Marble-Hosted Wollastonite Deposit at Bi'r Ash Shumt, Kingdom of Saudi Arabia," *Earth Sciences Journal,* vol. 3, pp. 129-144, 1990.

[44]. P. Nehlig, I. Salpeteur, F. Asfirane, V. Bouchot, J. Eberlé, and A. Genna, "The mineral potential of the Arabian shield: a reassessment," in *Proceedings of the IUGS/UNESCO Meeting on the "Base and Precious Metal Deposits in the Arabian Shield", Jeddah, November*, 1999, pp. 12-19.

[45]. F. Robinson, J. Foden, and A. Collins, "Geochemical and isotopic constraints on island arc, synorogenic, post-orogenic and anorogenic granitoids in the Arabian Shield, Saudi Arabia," *Lithos,* vol. 220, pp. 97-115, 2015.

[46]. W. J. Hinze, R. R. Von Frese, R. Von Frese, and A. H. Saad, *Gravity and magnetic exploration: Principles, practices, and applications*: Cambridge University Press, 2013.

[47]. A. M. Eldosouky, H. Sehsah, S. O. Elkhateeb, and A. B. Pour, "Integrating aeromagnetic data and Landsat-8 imagery for detection of post-accretionary shear zones controlling hydrothermal alterations: The Allaqi-Heiani Suture zone, South Eastern Desert, Egypt," *Advances in Space Research,* vol. 65, pp. 1008-1024, 2020.

[48]. H. Sehsah and A. M. Eldosouky, "Neoproterozoic hybrid forearc–MOR ophiolite belts in the northern Arabian-Nubian Shield: no evidence for back-arc tectonic setting," *International Geology Review,* vol. 64, pp. 151-163, 2022.

[49]. H. Sehsah, A. M. Eldosouky, and A. H. El Afandy, "Unpaired ophiolite belts in the Neoproterozoic Allaqi-Heiani Suture, the Arabian-Nubian Shield: evidences from magnetic data," *Journal of African Earth Sciences,* vol. 156, pp. 26-34, 2019.

[50]. L. T. Pham, A. M. Eldosouky, E. Oksum, and S. A. Saada, "A new high resolution filter for source edge

detection of potential field data," *Geocarto International,* vol. 37, pp. 3051-3068, 2022.

[51]. Geosoft, "Magmap filtering how-to guide: defining and applying filters and inverse FFT in MagMap," p. 23, 2015.

[52]. M. N. Nabighian, "The analytic signal of two-dimensional magnetic bodies with polygonal cross-section: its properties and use for automated anomaly interpretation," *Geophysics,* vol. 37, pp. 507-517, 1972.

[53]. A. Salem, D. Ravat, T. J. Gamey, and K. Ushijima, "Analytic signal approach and its applicability in environmental magnetic investigations," *Journal of Applied Geophysics,* vol. 49, pp. 231-244, 2002.

[54]. A. Salem and D. Ravat, "A combined analytic signal and Euler method (AN-EUL) for automatic interpretation of magnetic data," *Geophysics,* vol. 68, pp. 1952-1961, 2003.

[55]. A. Salem, S. Williams, J. D. Fairhead, D. Ravat, and R. Smith, "Tilt-depth method: A simple depth estimation method using first-order magnetic derivatives," *The leading edge,* vol. 26, pp. 1502-1505, 2007.

[56]. M. Reford and J. Sumner, "Aeromagnetics," *Geophysics,* vol. 29, pp. 482-516, 1964.

[57]. M. T. Einaudi and D. M. Burt, "Introduction; terminology, classification, and composition of skarn deposits," *Economic geology,* vol. 77, pp. 745-754, 1982.

[58]. J. M. Hammarstrom, B. B. Kotlyar, T. G. Theodore, J. E. Elliott, D. A. John, J. L. Doebrich*, et al.*, "Cu, Au, and Zn-Pb Skarn Deposits," *Preliminary Compilation of Descriptive Geoenvironmental Mineral Deposit Models, US Geological Survey Open-File Report,* pp. 95-831, 1995.

[59]. P. R. Whitney and J. F. Olmsted, "Rare earth element metasomatism in hydrothermal systems: The Willsboro-Lewis wollastonite ores, New York, USA," *Geochimica et Cosmochimica Acta,* vol. 62, pp. 2965-2977, 1998.

[60]. U. Ghosh and D. Upadhyay, "The retrograde evolution of F-rich skarns: Clues from major and trace element chemistry of garnet, scheelite, and vesuvianite from the Belka Pahar wollastonite deposit, India," *Lithos,* vol. 422, p. 106750, 2022.

[61]. F. Cocco, A. Attardi, M. L. Deidda, D. Fancello, A. Funedda, and S. Naitza, "Passive structural control on skarn mineralization localization: a case study from the Variscan Rosas Shear Zone (SW Sardinia, Italy)," *Minerals,* vol. 12, p. 272, 2022.

[62]. T. Baker and J. R. Lang, "Reconciling fluid inclusion types, fluid processes, and fluid sources in skarns: an example from the Bismark Deposit, Mexico," *Mineralium Deposita,* vol. 38, pp. 474-495, 2003.

[63]. P. Deb, D. Knapp, G. Marquart, C. Clauser, and E. Trumpy, "Stochastic workflows for the evaluation of Enhanced Geothermal System (EGS) potential in geothermal greenfields with sparse data: the case study of Acoculco, Mexico," *Geothermics,* vol. 88, p. 101879, 2020.

[64]. R. H. Sillitoe and H. F. Bonham Jr, "Sediment-hosted gold deposits: Distal products of magmatic-hydrothermal systems," *Geology,* vol. 18, pp. 157-161, 1990.

[65]. C. L. Ciobanu and N. J. Cook, "Skarn textures and a case study: the Ocna de Fier-Dognecea orefield, Banat, Romania," *Ore Geology Reviews,* vol. 24, pp. 315-370, 2004.

[66]. M. Yousefi and J. M. Hronsky, "Translation of the function of hydrothermal mineralization-related focused fluid flux into a mappable exploration criterion for mineral exploration targeting," *Applied Geochemistry,* vol. 149, p. 105561, 2023.

[67]. S. M. Heidari, P. Afzal, and B. Sadeghi, "Molybdenum and gold distribution variances within Iranian copper porphyry deposits," *Journal of Geochemical Exploration,* vol. 261, p. 107471, 2024.

[68]. P. Kianoush, N. Keshavarz Faraj Khah, P. Afzal, E. Jamshidi, A. H. Bangian Tabrizi, and A. Kadkhodaie, "Formation Pressures Determination Utilizing the Integration of Fractal and Geostatistical Modelling in a Hydrocarbon Formation of SW Iran," *Journal of Analytical and Numerical Methods in Mining Engineering,* 2024.

[69]. M. M. Pourgholam, P. Afzal, A. Adib, K. Rahbar, and M. Gholinejad, "Delineation of Iron alteration zones using spectrum-area fractal model and TOPSIS decision-making method in Tarom Metallogenic Zone, NW Iran," *Journal of Mining and Environment,* vol. 13, pp. 503-525, 2022.

[70]. M. Zamyad, P. AFZAL, M. POURKERMANI, R. NOURI, and M. R. JAFARI, "Combination of Spectral Feature Fitting (SFF) and Concentration-Number (CN) Fractal Modeling for Identification Alteration in Tirka Area, NE Iran," 2022.

[71]. K. Mostafaei, M. N. Kianpour, and M. Yousefi, "Delineation of Gold Exploration Targets based on Prospectivity Models through an Optimization Algorithm," *Journal of Mining and Environment,* vol. 15, pp. 597-611, 2024.

[72]. M. Saremi, S. Yousefi, and M. Yousefi, "Combination of Geochemical and Structural Data to Determine Exploration Target of Copper Hydrothermal Deposits in Feizabad District," *Journal of Mining and Environment,* vol. 15, pp. 1089-1101, 2024.

[73]. A. D. Ettlinger, L. D. Meinert, and G. E. Ray, "Gold skarn mineralization and fluid evolution in the

Nickel Plate Deposit, British Columbia," *Economic Geology,* vol. 87, pp. 1541-1565, 1992.

[74]. Z. Chang and L. D. Meinert, "Zonation in skarns and the controlling factors," *TUNGSTEN, FIRE AND ICE IN THE REALM OF THE ANCIENT KING,* p. 35, 2009.

[75]. D. R. Cooke, C. L. Deyell, P. J. Waters, R. I. Gonzales, and K. Zaw, "Evidence for magmatic-hydrothermal fluids and ore-forming processes in epithermal and porphyry deposits of the Baguio district, Philippines," *Economic Geology,* vol. 106, pp. 1399-1424, 2011.

[76]. D. P. Braxton, D. R. Cooke, A. M. Ignacio, and P. J. Waters, "Geology of the Boyongan and Bayugo porphyry Cu-Au deposits: An emerging porphyry district in northeast Mindanao, Philippines," *Economic Geology,* vol. 113, pp. 83-131, 2018.

[77]. W. Ma, Y. Liu, Z. Yang, Z. Li, X. Zhao, and F. Fei, "Alteration, mineralization, and genesis of the Lietinggang–Leqingla Pb–Zn–Fe–Cu–Mo skarn deposit, Tibet, China," *Ore Geology Reviews,* vol. 90, pp. 897-912, 2017.

[78]. J. A. Fitzherbert, A. R. McKinnon, P. L. Blevin, K. Waltenberg, P. M. Downes, C. Wall*, et al.*, "The Hera orebody: A complex distal (Au–Zn–Pb–Ag–Cu) skarn in the Cobar Basin of central New South Wales, Australia," *Resource Geology,* vol. 71, pp. 296-319, 2021.

پیشنهادی برای رسوبات جدید اسکارن پرکامبرین در سپر عربی

عید ر. ابوعز[۱،۲]، السید اول سلیم[۱،۳]، حاتم ابوالخیر[۳،۴]، و هیثم صحصح[۳]*

۱- گروه فیزیک، دانشکده علوم و علوم انسانی، دانشگاه شاهزاده سطام بن عبدالعزیز، ۱۱۹۴۲، الخرج، عربستان سعودی

۲- گروه ژئوفیزیک، دانشکده علوم، دانشگاه قاهره، جیزه، P.O. 12613، مصر

۳- دانشکده علوم، گروه زمین شناسی، دانشگاه دامیتا، شهر جدید دامیتا، ۳۴۵۱۷، مصر

۴- مرکز تحقیقات و کاربردهای فضایی (CSRA)، دانشگاه دامیتا، شهر جدید دمیتا، مصر

ارسال ۲۰۲۴/۰۶/۱۵، پذیرش ۲۰۲۴/۰۸/۰۴

* نویسنده مسئول مکاتبات: Haytham_sehsah@du.edu.eg

چکیده:

هیپسومتری دووجهی سپر عربی-نوبی در نئوپروتروزوئیک باعث تشکیل حوضه های دریایی پس از ادغام در زمین های کم ارتفاع سپر عربی (ع) شد. توالی‌های کربناته در حوضه‌های دریایی خارق‌العاده در AS توسط توده‌های گرانیتی از انواع مسبب مختلف، با مسیرهای مناطق برشی عمده نفوذ می‌کنند. بنابراین، شرایط برای تشکیل رسوبات اسکارن در تماس توالی کربناته با توده های گرانیتی ایجاد می شود. رویکردهای چند رشته‌ای از جمله داده‌های ASTER، داده‌های مغناطیسی و داده‌های ژئوشیمیایی در حوضه مرداما برای تعیین مکان‌های امیدوارکننده برای رسوبات اسکارن اعمال شده‌اند. حوضه مرداما دارای ناهنجاری های مغناطیسی متضاد با شدت های مختلف در تماس بین سنگ آهک مرداما و باتولیت های مسبب پس از مرداما است. ناهنجاری های مغناطیسی قابل توجهی در تماس با ماگماهای ایجاد کننده آیدا وجود دارد. خطوط خطی مربوط به سیستم گسلی نجد (NFS) به سمت شرق وجود دارد، جایی که کانی‌های مرتبط با دگرسانی کلک سیلیکات تکامل یافته‌اند، بدون هیچ سرنخی برای اثر نفوذ برای چنین فعالیت دگرسانی در طول مسیرهای مربوط به سیستم شکستگی یا در تماس با مجموعه آبانات. تکنیک‌های مختلف نقشه‌برداری طیفی، از جمله واگرایی اطلاعات طیفی (SID)، نقشه‌برداری زاویه طیفی (SAM) و کمینه‌سازی انرژی محدود (CEM) تأیید می‌کنند که مجموعه آیدا ماگمای مسبب غالب در منطقه مورد مطالعه با تغییرات کالک سیلیکات بسیار تکامل یافته است. مواد معدنی مانند ولاستونیت، گارنت و پیروکسن. در همین حال، سوئیت آیدا به عنوان ماگمای عامل اصلی برای سایر مناطق کاهش یافته اسکارن که از حوضه مرداما، یعنی کیتان و آن نیمریه جنوبی ثبت شده اند، شناسایی شده است. مناطق معدنی مرتبط با دگرسانی کائولینیت، کلریت، مسکویت و هماتیت همراه با کانی‌های کالک سیلیکات در محل تماس بین Idah و عضو کربنات مرداما تکامل یافته‌اند. داده‌های ژئوشیمیایی نشان‌دهنده کاهش اثر برای مجموعه آیدا در تماس بین توالی کربنات مرداما و توده‌های آیدا است. این نتایج اولیه از این مطالعه نیاز به تحقیقات میدانی دقیق و اکتشافات ژئوشیمیایی برای نهشته‌های اسکارن پیشنهادی در حوضه ملاس نئوپروتروزوییک AS دارد.

کلمات کلیدی: اسکارن نئوپروتروزوییک، کربنات مرداما، توده های عامل، سپر عربی-نوبی، حالت ردوکس ماگما.